Fatty Acid-Specific Fluorescent Probes and Their Use in Resolving Mixtures of Unbound Free Fatty Acids in Equilibrium with Albumin†

Andrew H. Huber,‡ J. Patrick Kampf,‡,§ Thomas Kwan,‡ Baolong Zhu,‡ and Alan M. Kleinfeld*,‡,§

FFA Sciences LLC and Torrey Pines Institute for Molecular Studies, San Diego, California 92121

Received April 11, 2006; Revised Manuscript Received July 6, 2006

ABSTRACT: We report the first measurements for profiling mixtures of unbound free fatty acids. Measurements utilized fluorescent probes with distinctly different response profiles for different free fatty acids (FFA). These probes were constructed by labeling site-specific mutants of the rat intestinal fatty acid binding protein (rI-FABP) with acrylodan. The probes were produced and screened by high-throughput methods, and from more than 30 000 such probes we selected six that together have sufficient specificity and sensitivity for resolving the profile of unbound FFA (FFA_u) in mixtures of different FFA_u. We developed analytical methods to determine the FFA_u profile from the fluorescence (ratio) response of the different probes and used these methods to determine FFA_u profiles for mixtures of arachidonate, linoleate, oleate, palmitate, and stearate in equilibrium with bovine serum albumin (BSA). Measurements were performed using mixtures with a range of total FFA_u concentrations, including 0.9 nM, which is similar to normal plasma levels. We also measured single FFA binding isotherms for BSA and found that binding was described well by six to seven sites with the same binding constants (K_d). The K_d values for the FFA (4−38 nM) were inversely related to the aqueous solubility of the FFA. We constructed a model with these parameters to predict the FFA_u profile in equilibrium with BSA and found excellent agreement between the profiles measured using the FFA probes and those calculated with this model. These results should lead to a better understanding of albumin's role in buffering FFA_u and to profiling FFA_u in intra- and extracellular biological fluids.

Metabolomics is advancing rapidly as a result of new technologies and the expanding interest in systems biology (*1*). This advance is being driven by the recognition that physiologic phenotype is essentially a reflection of the metabolic profile, and therefore, metabolic profiling should provide an accurate representation of the states of health and disease. The activity of a given metabolite is frequently dictated by its solubility as a "free" or unbound molecule in aqueous bodily fluids. For many metabolites, the unbound concentration represents a small fraction of the total, with most of the total metabolite bound in carrier complexes. Total metabolite concentrations are typically measured, but it is the unbound metabolite that interacts with targets such as protein receptors and cell membranes (for example, ref *2*). A profiling of unbound metabolite concentrations should therefore provide the most accurate measure of physiologic health.

The issue of profiling unbound rather than total metabolites is especially relevant for the long chain free fatty acids (FFA),[1] which play major roles in signaling, macromolecular structure, and energy production. Long chain FFA are sparingly soluble yet act through extra- and intracellular aqueous phases to bind to target macromolecules (*2*−*4*). In many instances, FFA-mediated signaling events can be abolished by adding fatty acid free bovine serum albumin, which reduces the unbound FFA (FFA_u)[2] concentration without changing the total FFA concentration (*8*, *9*). Total serum concentrations of long chain FFA are in the millimolar range, while FFA−protein receptor binding affinities are in the nanomolar range as are FFA_u concentrations (*4*−*7*). The hydrophobic nature of FFA and low FFA_u concentrations have made it difficult to measure FFA_u concentrations in biological fluids, and thus, the total FFA concentration is typically measured even though FFA-dependent signaling events are triggered by unbound rather than total FFA concentrations.

† This work was supported by Grant DK070314 from the NIH Roadmap Initiative in Metabolomics Technology Development.

* To whom correspondence should be addressed: Torrey Pines Institute for Molecular Studies, 3550 General Atomics Ct., San Diego, CA 92121. Telephone: (858) 455-3724. Fax: (858) 455-3792. E-mail: akleinfeld@tpims.org.

‡ FFA Sciences LLC.

§ Torrey Pines Institute for Molecular Studies.

[1] Abbreviations: FABP, fatty acid binding protein; rI-FABP, rat intestinal FABP; ADIFAB, acrylodan-labeled rI-FABP; ADIFAB2, acrylodan-labeled L72A mutant of rI-FABP; BSA, bovine serum albumin; FFA, free fatty acids; FFA_u, unbound FFA; AA, arachidonic acid (20:4 Δ5,8,11,14); LNA, linolenic acid (18:3 Δ9,12,15); LA, linoleic acid (18:2 Δ9,12); OA, oleic acid (18:1 Δ9); SA, stearic acid (18:0); POA, palmitoleic acid (16:1 Δ9); PA, palmitic acid (16:0).

[2] FFA are nonesterified or "free" fatty acids, and "unbound FFA" are aqueous phase monomers of FFA, a state which can be detected by the probes. Because a fatty acid is, by definition, nonesterified, the term free fatty acid could be used to denote the unbound fatty acid. Nevertheless, the most common usage refers to nonesterified fatty acids as free fatty acids, primarily to distinguish fatty acids from fatty esters. Because few studies have dealt explicitly with the unbound, aqueous phase monomers, we have in this study and previous studies used FFA_u to emphasize the distinction between the unbound fatty acids in the aqueous phase and those that are protein- or lipid-bound.

10.1021/bi060703e CCC: $33.50
Published on Web 11/09/2006

More than 40 different species of FFA with widely different biological activities have been identified in human serum (*10*). Striking examples of their different biological activities include the induction of apoptosis in various cell types by palmitate (16:0) but not oleate (18:1) (*11*−*13*) and the inhibition of cytotoxic T lymphocyte signaling by oleate (OA) but not palmitate (PA) (*9*, *14*). In addition, alterations in the profile of total plasma FFA have been reported in association with disease states (*10*, *15*−*18*).

Plasma FFA_u levels are a reflection of the FFA−albumin binding equilibrium. The affinities of albumin for different FFA can differ by more than 2 orders of magnitude (*5*, *19*), and therefore, the equilibrium FFA_u profile will differ from the total profile. FFA_u profiles have not been reported previously because none of the available measurement techniques can resolve the nanomolar quantities of individual FFA_u in the FFA_u mixtures present in aqueous biological fluids. However, measurements of individual FFA_u and/or average values for FFA_u mixtures have been carried out previously using the acrylodan-labeled fatty acid binding proteins ADIFAB and ADIFAB2 (*7*, *20*).

In this study, we have developed new fluorescently labeled fatty acid binding proteins (probes) with FFA response profiles distinctly different from those of ADIFAB and ADIFAB2. Together, these new probes have sufficient specificity and sensitivity for resolving individual FFA_u in FFA_u mixtures. The new probes were constructed by labeling site-specific mutants of the rat intestinal fatty acid binding protein (rI-FABP) with acrylodan. More than 30 000 such probes were generated and screened for ligand specificity using high-throughput methods. We have selected and further characterized a subset of more than 140 probes that have high sensitivity and specificity for individual FFA. In this study, we describe six probes that display specificity for the five FFA that are among the most abundant in human plasma: PA, OA, linoleate (LA), stearate (SA), and arachidonate (AA).

As a first step toward the determination of blood plasma FFA_u profiles, we have used these six new probes to profile mixtures of four and five FFA in equilibrium with bovine serum albumin (BSA). Because there is no independent method for determining FFA_u concentrations, we also calculated the expected profiles from the known amounts of FFA and BSA used to generate the mixtures. These calculations required binding constants for each BSA−FFA interaction and a new BSA binding model. Our measurements indicate that, to a good approximation, the binding of each of the FFA to BSA can be described in terms of a single class of six to seven independent sites. Using this simple model, we have calculated FFA_u profiles for mixtures of four and five FFA in equilibrium with BSA and compared these predictions to FFA_u profiles measured with our probes. Good agreement was found between these two independent profiling methods.

EXPERIMENTAL PROCEDURES

Materials. Essentially fatty acid free bovine serum albumin, buffer salts, DNase I, lysozyme, HEPES, His-Select Ni-Affinity Gel, hydroxyalkoxypropyl dextran, *N*,*N*-dimethylformamide (DMF), and Triton X-100 were purchased from Sigma-Aldrich (St. Louis, MO). Fatty acid sodium salts were obtained from NuChek Prep (Elysian, MN). ADIFAB and ADIFAB2 were prepared as previously described (*21*, *22*) and are available from FFA Sciences LLC (San Diego, CA). Acrylodan was purchased from Invitrogen (Carlsbad, CA). Oligonucleotides were synthesized by Operon Biotechnologies, Inc. (Huntsville, AL). The protein expression vector (pET11d) for mutant rI-FABP was obtained from Novagen (Madison, WI). DNA modification enzymes were from Stratagene (La Jolla, CA) and New England Biolabs (Ipswich, MA). Protein Assay reagents were purchased from Bio-Rad (Hercules, CA).

The following buffers and stocks were used. Measurement buffer contained 20 mM HEPES, 140 mM NaCl, 5 mM KCl, and 1 mM Na_2HPO_4 (pH 7.4). Storage buffer was measurement buffer with 0.05% (w/v) sodium azide and 1 mM EDTA. Lysis buffer contained 50 mM Tris-HCl (pH 8), 250 mM NaCl, 5 mM $MgSO_4$, 5 mM KCl, 1.0 mg/mL lysozyme, and 5 μg/mL DNase I. Buffer 1 contained 50 mM Tris (pH 8.0), 200 mM NaCl, and 10 mM imidazole. Elution buffer contained 15 mM HEPES (pH 7.4), 110 mM NaCl, 4 mM KCl, 1 mM Na_2HPO_4, and 100 mM EDTA. BTP buffer contained 10 mM Bis-Tris propane (pH 9.3) and 100 mM NaCl. Buffer 2 contained 50 mM Tris (pH 8.0), 200 mM NaCl, and 15 μM essentially fatty acid free BSA. Buffer 3 contained 10 mM Tris (pH 8.0) and 200 mM NaCl. Buffer 4 contained 50 mM Tris-HCl, 5 mM $MgCl_2$, and 200 mM NaCl (pH 8). Buffer 5 contained 75 mM Tris-HCl (pH 8.0), 150 mM NaCl, and 250 mM imidazole. Buffer 6 contained 10 mM BTP (pH 9.3) and 50 mM NaCl. All acrylodan stocks were prepared in DMF.

Library Generation. Libraries of mutant rI-FABP proteins were created by in vitro site-directed mutagenesis using a PCR overlap extension method (*23*). All mutant FABP genes had an E131D mutation plus a COOH-terminal Arg-Gly-six-histidine tag. NcoI and BamHI restriction sites were added to 5′- and 3′-ends of the tagged FABP gene by incorporating them into the 5′- and 3′-terminal oligonucleotides for PCR. The NcoI- and BamHI-digested library was ligated into the NcoI- and BamHI-digested pET-11d- vector, and *Escherichia coli* strain BL21(DE3) was transformed with the ligation mixture. Transformed cells were plated onto Luria-Broth agar containing 100 μg/mL carbenicillin (LB/carb agar).

Library Prescreening. Isolated colonies were picked for small-scale growth in 96-position deep-well plates containing 375 μL of LB/carb per well. Cultures were grown overnight and induced the next morning by adding 125 μL of a 1.6 mM solution of IPTG in LB/carb. After an additional 4 h at 37 °C, the cells were pelleted by centrifugation and the pellets stored at −80 °C.

Cells were lysed by adding 200 μL of lysis buffer to each thawed pellet and subjecting the cells to two freeze−thaw cycles. Cellular debris was pelleted by centrifugation, and 150 μL of lysate supernatant from each well was transferred to a fresh deep-well block. Approximately 30 μL of a 25% suspension of His-Select Ni-Affinity Gel was added to each well, the mixture incubated for 10 min at room temperature, and the lysate aspirated away. Each bed of Ni affinity beads was washed once with a 1.4 mL aliquot of buffer 1. Affinity-purified protein was eluted by adding 50 μL of elution buffer to each well and incubating the mixtures at room temperature for 10 min. Eluted protein concentrations were estimated

using the Bio-Rad protein assay (*24*). Clones with suitable levels of protein expression were chosen for additional characterization.

Small-Scale Purification and Labeling of Mutant FABP. Clones yielding sufficient protein during prescreening were grown overnight in 48-position deep-well plates, with each well containing 1.5 mL of LB/carb. Cultures were induced the next morning by adding 1.5 mL of an 800 μM solution of IPTG in LB/carb. After an additional 4 h at 37 °C, the cells were pelleted by centrifugation and the pellets stored at −80 °C.

Cells were lysed by adding 200 μL of lysis buffer to each thawed pellet and subjecting the samples to two freeze−thaw cycles. Cellular debris was pelleted by centrifugation, and 200 μL of lysate supernatant from each well was transferred to a fresh deep-well block. The lysate from pairs of 48-position blocks was moved to single 96-position deep-well blocks for labeling.

Approximately 100 μL of a 25% slurry of His-Select Ni-Affinity Gel was added to each well, the mixture incubated 10 min at room temperature, and the lysate discarded. The bed of Ni affinity beads in each well was washed once with 1.4 mL of buffer 1 and three times with 1.4 mL aliquots of BTP buffer. The addition of 500 μL of 37 °C BTP buffer followed by 5 μL of 20 mM acrylodan to each well started the labeling reaction. Samples were incubated for 1 h at 37 °C with end-over-end mixing. The beads in each well were washed once with 1.4 mL of buffer 2 and three times with 1.4 mL aliquots of buffer 3. Mutant FABP probes were eluted at room temperature with 250 μL aliquots of elution buffer. Probe concentrations were estimated using the Bio-Rad protein assay.

Large-Scale Purification and Labeling of Mutant FABP. Cultures in LB/carb were grown in baffled shake flasks at 37 °C and induced during late log phase by adding IPTG to a final concentration of 200 μM. Cells were harvested by centrifugation 3 h after induction and stored at −80 °C. Cell pellets were resuspended in 7 mL of buffer 4/g of cells, and protease inhibitors (2.6 mg of phenylmethanesulfonyl fluoride and 28 μg of aprotinin per gram of cell pellet) were added to the suspension. DNase I and Triton X-100 were added to final concentrations of 8.75 μg/mL and 1% (v/v), respectively. Cellular debris was pelleted and the lysate supernatant passed over a His-Select HF Nickel Affinity column. Purified FABP was eluted with buffer 5. Additional size exclusion and anion exchange chromatography steps provided pure mutant FABP.

Fluorescent probes were generated by slowly adding 20 mM acrylodan to a 100 μM FABP stock in buffer 6 until an acrylodan:protein molar ratio of 2:1 was reached. The reaction mixture was incubated at 37 °C with constant mixing for the duration of the acrylodan addition and for 1 h afterward. Placing the reaction vessel on ice and neutralizing the reaction pH with HCl terminated the reaction. Unreacted acrylodan was removed with a hydroxyalkoxypropyl dextran column, and the probe was further purified by size exclusion chromatography, using an XK 26/100 Superdex 200 Prep-grade column (GE Healthcare components) equilibrated with measurement buffer. The labeling efficiency of monomer peak fractions was checked by reversed phase column chromatography (Grace-Vydac, 214MS54-C4) and by measuring fluorescence R values (see eq 1). Suitable fractions were pooled to create a final probe stock. EDTA and sodium azide were added as preservatives at final concentrations of 1 mM and 0.05% (w/v), respectively.

Phenotypic Screening. Probe FFA_u response profiles (phenotypes) were determined in a 384-well format by measuring the fluorescence response of each probe to seven different FFA. Screening success was critically dependent upon the preparation of FFA solutions with precisely defined and highly reproducible unbound concentrations ($[FFA_u]$). To avoid pitfalls resulting from the low solubility of long chain fatty acids and their propensity for nonspecific binding to surfaces, BSA was used as a buffering agent. Reliable $[FFA_u]$ values were generated by using FFA−BSA complexes as described previously (*3*). FFA−BSA complexes were prepared by slow addition of alkaline (pH >11) stocks of 50 mM fatty acid sodium salts to stirred solutions of 600 μM BSA in measurement buffer at 37 °C. FFA sodium salts were used because they dissolve more rapidly than the neat acid. The alkaline stocks of PA and SA were warmed to 70 °C before addition to the BSA solution as described in ref *25*. Desired stock FFA_u concentrations, which ranged from 10 to 1500 nM depending on the FFA type, were achieved through an iterative process of fatty acid addition and measurement of $[FFA_u]$ with ADIFAB2. The complexes were diluted to 12 and 6 μM BSA in measurement buffer for screening and measurement with ADIFAB2, respectively.

The fluorescence ratio (R) of each well in the 384-well plate was measured at emission wavelengths of 457 and 550 nm upon excitation at 375 nm. R is defined by eq 1

$$R = \frac{I_{550}^{\text{Probe}} - I_{550}^{\text{Blank}}}{I_{457}^{\text{Probe}} - I_{457}^{\text{Blank}}} \quad (1)$$

where I_λ^{Probe} is the intensity of the well at emission wavelength λ (nanometers) with a probe present and I_λ^{Blank} is the intensity without a probe present (*21*). Emission wavelengths of 457 and 550 nm were chosen to minimize the effects of absorption by hemoglobin on R, which is necessary for profiling FFA_u in blood, a future use for these probes (*7*, *26*). The absorbance of hemoglobin is equivalent at each of the two wavelengths and will offset in R. Each screening well contained 0.5−10 μM probe and either fatty acid free BSA or the FFA−BSA complex in 0.1 mL of measurement buffer. The magnitude of the ratio measurement error depended upon probe intensity and was typically ≤2%.

With each probe, the difference (ΔR) between the ratio with and without each fatty acid was determined and compared to that for the reference probe ADIFAB2 (ΔR_{AD2}) by dividing the ratio changes ($\rho_i \equiv \Delta R/\Delta R_{AD2}$). The set of ρ_i for all FFA screened defined the phenotype for a given probe. Probes for which all ρ_i values were close to 1 had responses similar to that of ADIFAB2 and were generally not characterized further. Likewise, probes for which all ρ_i values were close to 0 were not useful FFA probes because they were not responsive to the screened FFA. Probes that exhibited significantly nonuniform ρ_i profiles were prepared on a larger scale, and a detailed characterization of their FFA binding and spectral properties was performed.

Probe Calibration. A complete calibration of each probe chosen for large-scale preparation was performed, at 22 °C, to determine the dissociation and fluorometric constants of

eq 2 which relates $[FFA_u]$ to R.

$$[FFA_u] = K_d Q \frac{R - R_0}{R_m - R} \quad (2)$$

where R_0 is the value of R when no FFA is present, Q is the ratio of the intensity at 457 nm when no FFA is present to that when the probe is saturated with FFA, K_d is the dissociation constant, and R_m is R at saturation. Probe calibration was a two-step process involving the titration of probes with (i) unbuffered and (ii) BSA-buffered FFA stocks with known total ($[FA_t] = [FFA_{bound}] + [FFA_u]$) and unbound FFA concentrations, respectively. The unbuffered titrations were performed as previously described (*21*, *27*). Briefly, R was measured as a 1 μM probe solution was titrated to saturation with small aliquots of a 100−250 μM FFA stock. The emission spectra of each probe were also recorded during titration with FFA to assess the spectroscopic change corresponding to the bound and free forms of the probe.

For a fully labeled probe, such as ADIFAB, a nonlinear fit to the titration data reveals the full set of fluorometric constants. Mutant probe preparations often had significant amounts of an unlabeled protein. In these cases, the effective FFA concentration for the titration was unknown because the affinity of the unlabeled protein was unknown, and therefore, an accurate determination of K_d was not possible. However, an accurate [FFA] was not needed to determine Q and R_m, and these values were determined from the first calibration step.

In the second step, the buffering properties of BSA were exploited to complete the calibration. A series of FFA−BSA complexes with increasing $[FFA_u]$ values (from 1 nM to 4 μM as determined by ADIFAB2) were prepared for each FFA as described above. The complexes were then diluted 100-fold in measuring buffer containing 0.5 μM probe, and R was measured for each complex. Because BSA buffers $[FFA_u]$, the presence of unlabeled protein did not alter $[FFA_u]$ as long as the albumin concentration was significantly greater than the protein concentration. Therefore, the resulting R versus $[FFA_u]$ data were used to accurately determine K_d for a fixed Q. At least two calibrations with each of the seven FFA were performed for each probe. The accuracy of the calibrations was checked with defined FFA−BSA complexes prior to the mixture measurements, and small corrections were made when necessary.

FFA−BSA Binding Isotherms. The binding affinities of individual FFA for BSA were determined using ADIFAB2 as previously described for ADIFAB (*5*). ADIFAB2 has approximately 10-fold higher affinities than ADIFAB and therefore provides more accurate $[FFA_u]$ values at low concentrations. Small aliquots of a 0.25−1 mM FFA solution were added to continuously stirred measurement buffer containing 1−6 μM albumin and 0.25−0.5 μM ADIFAB2 at 22 °C. The fluorescence ratio was measured following each addition, from which $[FFA_u]$ was determined using eq 2. The amount of FFA bound to albumin was calculated by subtracting the amount of unbound FFA and FFA bound to ADIFAB2 (*5*) from the total amount of FFA added.

Resolving Mixtures of Fatty Acids. Albumin−FFA mixtures with a defined total $[FFA_u]$ ($=\sum_{i=1}^{n}[FFA_{ui}]$) were obtained by mixing together different volumes of single FFA−BSA complexes, each with $[FFA_u]$ equal to the desired total $[FFA_u]$. For example, to make a 1:1:1 tertiary mixture of LA, OA, and PA at a total FFA_u concentration of 4 nM, we mixed together equal portions of individual LA−BSA, OA−BSA, and PA−BSA complexes, each with an FFA_u concentration of 4 nM. Although equal volumes of the complexes were mixed, the FFA_u distribution was not uniform because each FFA has a different binding affinity for albumin.

FFA_u measurements for the FFA−BSA mixtures were taken with a suite of probes having different FFA specificities. Profiling requires measurement with at least one probe per FFA species. The response, R, of a probe to a sample with multiple FFA is described by eq 3

$$\sum_{i=1}^{n} \frac{[FFA_{ui}]}{Q_i K_{di}} (R_{mi} - R) = R - R_0 \quad (3)$$

where R_0, R_{mi}, Q_i, and K_{di} are probe spectral and binding constants as described in the previous section and the subscript i denotes the different FFA.

Equation 3 is an extension of eq 2, which describes the response of a single probe to a single fatty acid. Profiling mixtures with multiple probes requires a set of equations, linear in $[FFA_{ui}]$, that describe the response of each probe to the mixture of FFA. This set of equations can be expressed in matrix form (eq 4)

$$\begin{bmatrix} \frac{R_{m1a}-R_a}{Q_{1a}K_{d1a}} & \frac{R_{m2a}-R_a}{Q_{2a}K_{d2a}} & \frac{R_{m3a}-R_a}{Q_{3a}K_{d3a}} & \cdots & \frac{R_{mna}-R_a}{Q_{na}K_{dna}} \\ \frac{R_{m1b}-R_b}{Q_{1b}K_{d1b}} & \frac{R_{m2b}-R_b}{Q_{2b}K_{d2b}} & \frac{R_{m3b}-R_b}{Q_{3b}K_{d3b}} & \cdots & \frac{R_{mnb}-R_b}{Q_{nb}K_{dnb}} \\ \frac{R_{m1c}-R_c}{Q_{1c}K_{d1c}} & \frac{R_{m2c}-R_c}{Q_{2c}K_{d2c}} & \frac{R_{m3c}-R_c}{Q_{3c}K_{d3c}} & \cdots & \frac{R_{mnc}-R_c}{Q_{nc}K_{dnc}} \\ \vdots & \vdots & \vdots & \ddots & \vdots \\ \frac{R_{m1z}-R_z}{Q_{1z}K_{d1z}} & \frac{R_{m2z}-R_z}{Q_{2z}K_{d2z}} & \frac{R_{m3z}-R_z}{Q_{3z}K_{d3z}} & \cdots & \frac{R_{mnz}-R_z}{Q_{nz}K_{dnz}} \end{bmatrix} \begin{bmatrix} [FFA_{u1}] \\ [FFA_{u2}] \\ [FFA_{u3}] \\ \vdots \\ [FFA_{un}] \end{bmatrix} = \begin{bmatrix} R_a - R_{0a} \\ R_b - R_{0b} \\ R_c - R_{0c} \\ \vdots \\ R_z - R_{0z} \end{bmatrix} \quad (4)$$

where subscripts *a*, *b*, *c*, etc., refer to different probes and subscripts *1*, *2*, *3*, etc., refer to different FFA. The matrix can be expanded to include any number of FFA (n) or probes (z) where $z \geq n$. The $[FFA_{ui}]$ distribution within a mixture was determined by measuring the response, R, of each probe and solving eq 4. We estimated the errors in the $[FFA_{ui}]$ values assuming a 1% error in the R values and calculated the resulting $[FFA_{ui}]$ using eq 4. This estimation yields uncertainties in $[FFA_{ui}]$ that ranged between 1 and 30% (see Table 6) and is thought to be conservative because the uncertainties in R are less than 1%.

Fluorescence Instrumentation. Probe calibrations, preparation of FFA−BSA complexes, and determination of FFA−BSA binding isotherms were performed on either an SLM 8100 or a Spex Fluorolog-3 spectrofluorometer. Phenotypic screening was completed on a Spex MicroMax 384 fluorescence plate reader. A custom-insulated chamber with circulating cold water was used to maintain a temperature of 22 ± 1 °C within the plate reader.

Measurements used to resolve mixtures of FFA were performed with a hand-held ratio fluorometer, the "FFA_u Meter" (FFA Sciences LLC), designed specifically for use with ADIFAB2 and analogous probes. This instrument uses an epifluorescence configuration and cylindrical glass cu-

Table 1: FFA Screening Profiles for Probes[a]

	ρ_i							
	AA	LNA	LA	OA	PA	POA	SA	mutations
L1P8 H2	−4.17	−4.78	−3.93	−5.38	−1.24	−2.73	−2.29	Y14M, L38M, L72W
L2P22 G6	3.70	6.73	5.15	3.27	5.88	8.13	1.12	M18I, G31Y, L72A, A73G
L10P7 A4	10.9	10.5	8.90	5.27	2.73	7.51	1.17	Y14L, M18L, G31Y, L72A, A73L, Y117A
L11P7 B3	8.50	7.99	7.73	9.23	5.33	7.10	6.50	M21F, L72A, L78V, L102V
L13P7 B4	4.42	3.36	3.24	3.62	0.87	2.98	0.50	L72A, R106W, Q115C
L18P5 G12	11.5	15.8	14.0	8.91	2.76	9.98	2.49	Y14R, M18L, A73F, Y117D

[a] Response profiles (ρ_i) for each of the six probes which were generated by three to six amino acid (using single-letter notation) substitutions in the wild-type rat intestinal FABP.

vettes containing sample volumes of 200 μL. A light-emitting diode provides excitation at 375 nm, and two photodiodes detect emission through bandpass filters, centered at 457 and 550 nm. FFA_u Meter measurements used 200 μL of measurement buffer, 1.5 μM probe, and 1% by volume of the FFA−BSA mixture. The ratio (R) was measured three times, and the average values were used with eq 4 to determine the [FFA_{ui}] distribution. The average standard deviation in the ADIFAB2 ratio using this instrument was 0.3%.

RESULTS

FFA Specificities of Mutant Probes. Screening approximately 30 000 mutant probes with seven different FFA yielded a large number of probes with novel phenotypes, and we chose approximately 140 of these probes for detailed characterization. The FFA_u response profiles (ρ_i values) were used to select a subset of six probes with significantly different and complementary responses to individual FFA. This subset revealed improved specificity for OA, PA, SA, LA, and AA relative to the ADIFAB2 template. These probes, which have three to six substitutions in the cavity/portal regions of rat I-FABP, were used to resolve mixtures of four and five FFA in complex with BSA (Table 1).

The six probes have different fluorescence responses to FFA binding as indicated by their different emission spectra (Figure 1). With the exception of L1P8H2, binding of FFA to all of the probes revealed an emission red shift of 20−80 nm that resulted from an intensity decrease between 425 and 480 nm and either an increase or no change in intensity between 500 and 550 nm. The L1P8H2 probe exhibits a negative response (R value decreases upon FFA binding) characterized by a blue shift of 50 nm that reflects an intensity increase at ∼450 and a decrease at ∼515 nm. For all probes, the ratio (R) of the intensity at 550 nm to that at 457 nm provides a direct measure of the fraction of bound probe. Therefore, eq 2 can be used to determine the unbound FFA concentration from the measurement of R with a calibrated probe (Experimental Procedures). Probes were calibrated for each FFA (Table 2) by determining their binding affinities (K_d) and fluorescent parameters (R_0, Q, and R_m), as described in Experimental Procedures. The specificity and magnitude of the response of a particular probe to a given FFA reflect both binding and fluorescence parameters. For example, L10P7A4 has virtually identical K_d values for OA and LA, but the response to LA is greater because its Q and R_m values are substantially larger than those for OA.

Specificity is best gauged by rearranging eq 2 and comparing the calculated fractional change in R ($\Delta R/R_0$) between probes for each FFA_u. This was done using the calibration parameters of Table 2 for 1 nM FFA_u, and the results for the six mutant probes and ADIFAB2 reveal the range of specificities generated by the mutation and screening procedures (Figure 2). The results for each probe are displayed in order of FFA solubility, from the most (POA) to the least (SA) soluble FFA. As discussed previously (*21*, *22*), the ADIFAB2 response directly reflects the FFA solubility, revealing a monotonic increase in response from POA (1%/nM) to SA (20%/nM). In contrast, both L1P8H2 and L13P7B4 respond most to OA, L2P22G6 is most sensitive to PA, L10P7A4 responds almost equally well to AA and LA, and L18P5G12 exhibits LA specificity. Like ADIFAB2, L11P7B3 is most sensitive to SA but with a more than 4-fold stronger response.

Fatty Acid−BSA Binding Isotherms. BSA binding affinities, which are required for the BSA binding model, were measured for the five fatty acids, AA, LA, OA, PA, and SA, as well as POA and LNA. The dissociation constant (K_{di}^a) and the number of binding sites (M) for each FFA (Table 3) were determined using eq A5 as described in the Appendix. Binding isotherms represented as the concentration of fatty acid bound divided by the total albumin concentration as a function of [FFA_u] are shown in (Figure 3). In all cases, the binding isotherms reveal a sharp increase in the concentration of fatty acid bound at low FFA_u concentrations and asymptotic saturation at high FFA_u concentrations.

The results of this analysis indicate that a single-class model (Appendix) with six to seven binding sites provides an excellent description of binding of FFA to BSA (Figure 3). A two-class analysis does not improve the fit to the data and yields virtually identical affinities for both classes that are in turn equivalent to the affinities of the single-class model. Binding affinities increase with a decrease in the aqueous solubility of the FFA (Table 3). Small deviations from single-class fits appear at the highest FFA_u levels, possibly resulting from binding to additional low-affinity sites on albumin, nonspecific binding of FFA to the cuvette, or a combination of these events.

Binding of Mixtures of Different Fatty Acids with BSA. We used our new probes (Table 1 and Figure 2) to resolve the FFA_u distributions of mixtures of fatty acids in equilibrium with BSA. Measurements were performed using mixtures of four and five FFA interacting with BSA (Tables 4, 5, and 7). The measured distributions were compared with the predictions of the single-class BSA binding model, which are indicated as model in Tables 4, 5, and 7.

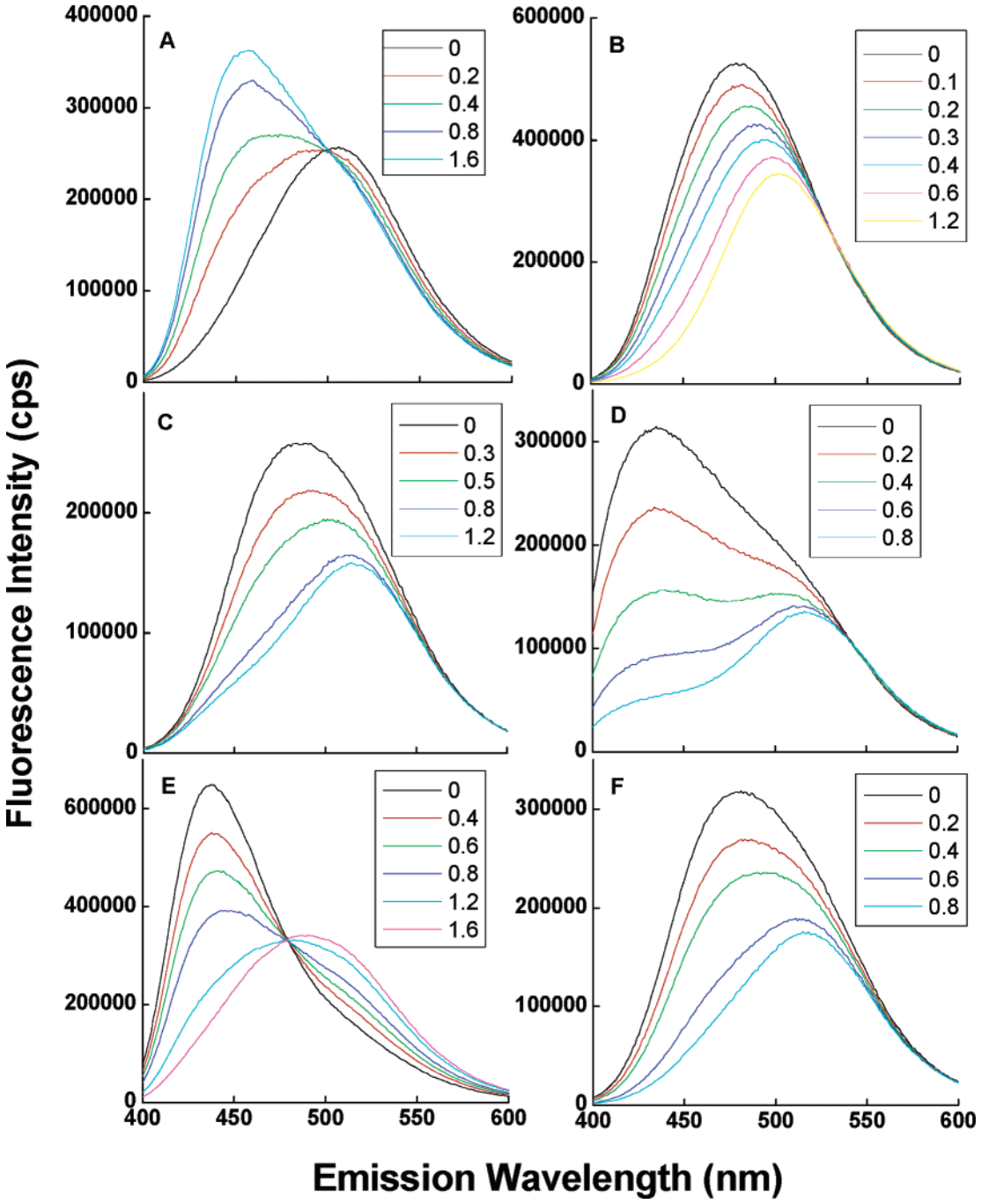

FIGURE 1: Fluorescence spectra of FFA-specific probes. The set of spectra for each probe represent titrations with increasing concentrations (in micromolar insets) of the FFA to which they best respond: (A) L1P8H2 with OA, (B) L2P22G6 with PA, (C) L10P7A4 with AA, (D) L11P7B3 with SA, (E) L13P7B4 with OA, and (F) L18P5G12 with LA. For all spectra, the excitation wavelength was 375 nm and the probe concentration was 1 μM.

Two separate mixtures (1:1:1:1 and 30:35:20:15) of the four FFA, AA, OA, PA, and SA, were used at total FFA_u concentrations of 3 and 20 nM. The FFA_u distributions resulting from the interaction of BSA with these two mixtures were resolved with the four probes L1P8H2, L2P22G6, L10P7A4, and L11P7B3. Excellent agreement was observed between measured and the model-predicted FFA_u distributions, which are presented as the concentration and the mole percent (X) of each FFA_u (Table 4). The average magnitude of the percentage difference between measured and model-predicted FFA_{ui} values was 10% (the average was −3%) with the largest difference (25%) occurring at the lowest-concentration component (SA at 0.31 nM).

Mixtures (1:1:1:1:1 and 20:25:30:15:10) of the five fatty acids, AA, LA, OA, PA, and SA, at total FFA_u concentrations of 3 and 20 nM were resolved using the probes L1P8H2, L2P22G6, L10P7A4, L11P7B3, and L18P5G12 (Table 5). Additional mixtures (1:1:1:1:1, 20:25:30:15:10, and 25:20:33:19:3) with a total FFA_u concentration of 0.9 nM were resolved using the L13P7B4 probe instead of L1P8H2 because L13P7B4 has better OA specificity than L1P8H2. The 25:20:33:19:3 mixture was chosen to approximate plasma FFA_u levels (*20*). These mixtures, comprising five FFA species, yielded profiles with the expected trends for the different FFA mixtures. The experimental uncertainties in the determination of the $[FFA_{ui}]$ values for these mixtures

Table 2: Probe Fluorescence Calibration Constants[a]

	L1P8 H2	L2P22 G6	L10P7 A4	L11P7 B3	L13P7 B4	L18P5 G12
R_0	0.62	0.20	0.69	0.29	0.09	0.49
K_d						
AA	104	90.6	5.1	248	35.9	47.5
LNA	217	89.0	13.9	249	149	13.1
LA	97.5	42.2	4.7	57.6	46.4	9.7
OA	14.4	33.9	4.9	20.1	10.5	20.0
PA	45.4	5.6	12.6	13.5	46.7	36.9
POA	209	87.9	22.3	176	90.3	90.7
SA	19.2	17.6	9.3	3.2	45.2	11.0
Q						
AA	0.24	2.80	1.89	4.70	2.19	4.39
LNA	0.27	3.75	2.31	5.61	1.83	5.26
LA	0.25	2.60	2.33	9.00	1.90	4.52
OA	0.20	2.37	1.60	6.70	2.17	3.57
PA	0.44	4.00	1.57	6.33	1.68	3.26
POA	0.47	2.73	1.87	5.10	1.78	4.15
SA	0.34	2.95	1.57	6.58	1.81	4.12
R_m						
AA	0.08	0.83	2.56	7.56	0.57	4.90
LNA	0.06	1.21	2.65	5.52	0.50	5.36
LA	0.08	0.99	2.59	5.94	0.52	6.50
OA	0.07	0.97	1.54	6.39	0.60	5.46
PA	0.17	1.21	1.60	4.10	0.24	3.82
POA	0.26	1.15	1.91	4.49	0.39	5.23
SA	0.12	0.87	1.36	6.02	0.43	3.98

[a] This table lists the binding (K_d) and spectroscopic (Q and R_m) parameters of eq 3 that determine the response of each of the probes to the different FFA.

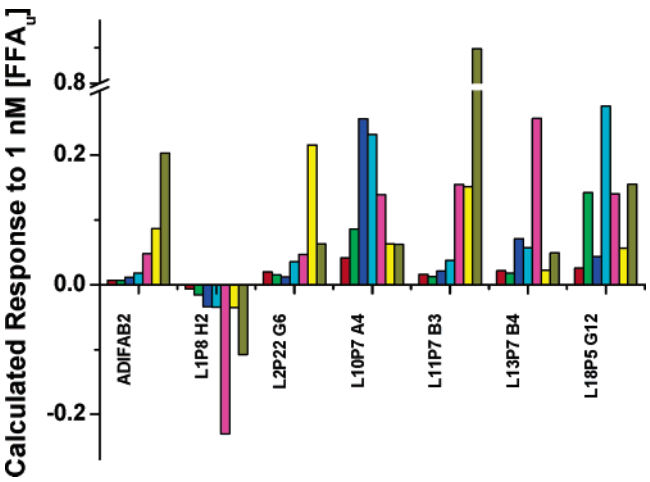

FIGURE 2: Probe response profiles. Profiles for each probe are represented as the fractional change in R for 1 nM FFA_u calculated using the calibration constants in Table 2. For each profile, the responses correspond from left to right to the most (POA) to least (SA) soluble FFA: red for POA, green for LNA, blue for AA, cyan for LA, pink for OA, yellow for PA, and brown for SA.

Table 3: Single-Class BSA−FFA Binding Parameters[a]

fatty acid	Ki_d^a (nM)	M	fatty acid	Ki_d^a (nM)	M
AA	16 ± 1	7.2 ± 0.6	PA	8.0 ± 0.2	6.9 ± 0.1
LNA	35 ± 1	7.2 ± 0.5	POA	38 ± 2	6.6 ± 0.5
LA	13 ± 2	7.3 ± 0.1	SA	4.1 ± 0.2	5.8 ± 0.3
OA	5.9 ± 0.1	7.4 ± 0.3			

[a] The binding parameters, binding constant ($K_{d_i}^a$), and number of binding sites (M), determined by fitting eq A5 to the BSA binding isotherms for single fatty acids.

were determined (Table 6) as described in Experimental Procedures and are representative of all the mixtures investigated in this study.

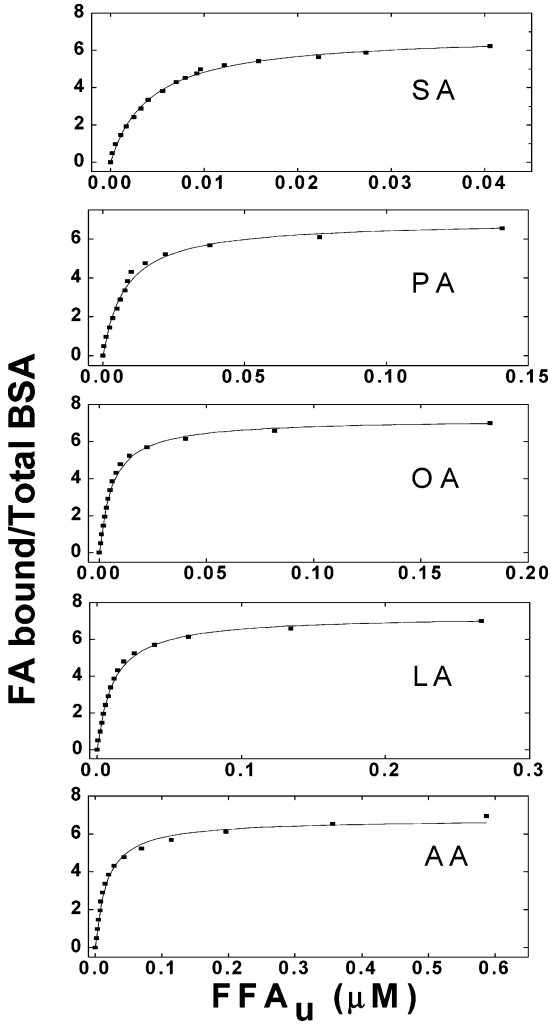

FIGURE 3: BSA binding isotherms for five different FFA. Measured FA bound/total BSA values are shown as solid square symbols, and the lines through these data represent best fits of the single-class albumin binding model. These results are representative of at least two separate titrations for each FFA.

The results also reveal excellent agreement between experiment and model distributions with average absolute values of the percentage differences ranging from 10% for the 3 and 20 nM mixtures to 13% for the 0.9 nM mixtures. The largest differences in [FFA_{ui}] between the experiment and model are for OA and PA in the 0.9 nM mixtures and partly reflect the estimated experimental uncertainties of Table 6 and the small dynamic range of the L13P7B4 probe (Table 2).

Differences in the FFA_u distributions for the different mixtures roughly follow the trend expected from the differences in binding affinities for BSA (Table 3). For the equal mixtures, [FFA_u] is largest for AA and smallest for SA, even though [FA_t] for SA is largest and that for AA is smallest (Table 7). As mentioned above, the [FFA_u] values for the single FFA−BSA complexes were the same before mixing. However, because SA has the highest affinity for BSA of the five FFA considered here, more SA needs to be added to the BSA for the stock to achieve the desired [FFA_u] value. The same [FFA_u] value is achieved with much less AA because it has the lowest affinity for BSA of the five FFA. For similar reasons, the relative fraction of AA tends to increase and that of SA decreases with an increasing total

Table 4: [FFA_u] Distributions Determined in Mixtures of Four Fatty Acids with BSA[a]

	1:1:1:1				30:35:20:15			
	experiment		model		experiment		model	
	[FFA_u] (nM)	*X* (%)	[FFA_u] (nM)	*X* (%)	[FFA_u] (nM)	*X* (%)	[FFA_u] (nM)	*X* (%)
AA	0.90	29	0.92	30	1.08	34	1.11	35
OA	0.81	26	0.72	23	1.21	39	1.01	32
PA	0.81	26	0.79	26	0.55	17	0.63	20
SA	0.58	19	0.67	22	0.31	10	0.40	13
total	3.10		3.10		3.15		3.15	
AA	7.75	39	7.70	39	9.45	46	9.10	45
OA	3.48	17	3.94	20	4.60	23	5.40	27
PA	5.32	27	4.97	25	4.54	22	3.90	19
SA	3.41	17	3.35	17	1.79	9	1.97	10
total	20.0		20.0		20.4		20.4	

[a] Experimental FFA_{ui} values were determined from two different mixtures (1:1:1:1 and 30:35:20:15) of AA, OA, PA, and SA by analyzing the measured probe responses with eq 4. The mixture ratios indicate the relative volume ratios of the FFA−BSA complexes used to prepare the mixtures (Experimental Procedures), and these are roughly the final [FFA_{ui}] ratios observed in the mixtures. Two concentrations of total FFA_u (3.1 and 20 nM) were used for each distribution. Model values of [FFA_{ui}] were calculated using the single-class model (eqs A4 and A6). Also shown is the fraction of each FFA_{ui} in the mixture (*X*).

[FFA_u]. For the most part, the differences in [FFA_u] distributions between the equal and 30:35:20:15 mixtures reflect the larger amounts of unsaturated (AA and OA) versus saturated (PA and SA) FFA_u in the mixtures.

DISCUSSION

We have developed high-throughput methods for generating large numbers of fluorescent probes derived from rI-FABP and for determining the FFA response profiles of the probes. A subset of probes with high specificity and sensitivity for different FFA was used to measure the distribution of FFA_u in BSA-buffered mixtures of some of the physiologically most abundant FFA. In addition, we determined the binding isotherms for single FFA interacting with BSA and used these results to formulate a single-class BSA binding model that accurately predicted the measured FFA_u distribution of equilibrated FFA−BSA mixtures. This is the first report of measurements that resolve unbound FFA concentrations in mixtures of different FFA, and our results suggest that it should be possible to measure the [FFA_u] profile in biologically relevant fluids.

Probe Generation and Screening. In previous studies, we measured the [FFA_u] of single FFA or the average [FFA_u] in mixtures of different FFA using two different fluorescent probes: ADIFAB (*21*) and ADIFAB2 (*7*, *22*, *26*). ADIFAB is fluorescently labeled wild-type rI-FABP, and ADIFAB2 is a fluorescently labeled L72A mutant. The L72A mutant was chosen from several that were tested (*28*, *29*) because the FFA binding affinities for the unlabeled protein were ~10-fold larger than for the wild-type protein. This difference was retained after fluorescent labeling, with ADIFAB2 binding affinities approximately 10-fold greater than those of ADIFAB. Moreover, the relative binding affinities and the relative fluorescence responses to different FFA were virtually identical for ADIFAB and ADIFAB2.

Unlike those of ADIFAB and ADIFAB2 (*28*, *29*), the fluorescence responses of most rI-FABP mutants are not simply correlated with the FFA binding affinities of the unlabeled proteins. For example, we did not predict from protein affinities that probes would reveal a negative response (L1P8H2) and that the fluorescence response of a given probe would be FFA-specific because the fluorescence parameters *Q* and R_{max} would be different for different FFA (Table 2). These results indicate that in searching for probes whose responses are specific for certain ligands, we must search using the probes rather than the unlabeled protein.

Single-Class Binding to BSA. Although the low solubility of long chain FFA and the rapid kinetics of their interactions with BSA place severe limitations on the types of methods that can be used, binding parameters for FFA interacting with BSA have been determined using several techniques (*5*, *19*, *30*−*35*). There is reasonable agreement among all studies that have reported BSA binding affinities after 1990, and these affinities are higher than those published in earlier studies (*30*). For example, in the studies of Bojesen and Bojesen (*31*, *33*, *34*), who assessed binding of PA, OA, LA, and AA to BSA at 23 °C with FFA:BSA ratios of up to 1.5, the results are consistent with a single class of three to four independent sites. Bojesen and Bojesen obtained K_d values at 23 °C for PA, OA, LA, and AA of 15, 3, 10, and 16 nM, respectively, which are reasonably similar to the respective values of 8, 6, 13, and 16 nM obtained in this study (Table 3). In addition, Rose et al. (*32*) and Elmadhoun et al. (*35*) both find good agreement with the stepwise BSA binding affinities published in our earlier study using ADIFAB (*5*).

In our previous study (*5*), we used ADIFAB to determine binding isotherms for long chain FFA interacting with BSA and analyzed the binding isotherms using the accepted stepwise model. We noted, however, that it was unclear whether the distinct binding constants for each of the six sites represented the actual binding constants (*5*). We have reanalyzed these earlier results and find that the single-class model yields a fit as good as that of the stepwise analysis (data not shown). These results are further supported by a more recent ADIFAB study in which we observed that binding of OA to BSA at 37 °C was described well by a single class of approximately five sites with a K_d of 14 nM (*36*). Moreover, we also measured dissociation rate constants for FFA−BSA complexes and found they were independent of the [FFA]:[BSA] ratio and that dissociation was consistent with a single rate constant (*36*). Rate constants were determined for PA, SA, OA, LA, LNA, and AA, and with the exception of LNA, the changes in k_{off} with FFA type correlate well with the changes in K_{di}^a with FFA type (Table 3). These equilibrium and kinetic results have shown that rate constants and equilibrium binding constants for FFA−BSA interactions are both consistent with single classes of multiple sites.

The accuracy of the FFA−BSA binding isotherms, and therefore the single-class model, depends directly on the accuracy with which FFA_u concentrations can be determined. The fluorescence probe method is quite simple, involving only the addition of probe to the FFA−BSA sample, a fluorescence measurement, and the calculation of the FFA_u concentration from the ratio of fluorescence intensities. We are not aware of any factors, other than those described in Experimental Procedures, that compromise the accuracy of our FFA_u measurements with ADIFAB2 or any other

Table 5: [FFA_u] Distributions Determined in Mixtures of Five Fatty Acids with BSA[a]

	1:1:1:1:1				20:25:30:15:10				25:20:33:19:3			
	experiment		model		experiment		model		experiment		model	
	[FFA_u] (nM)	*X* (%)	[FFA_u] (nM)	*X* (%)	[FFA_u] (nM)	*X* (%)	[FFA_u] (nM)	*X* (%)	[FFA_u] (nM)	*X* (%)	[FFA_u] (nM)	*X* (%)
AA	0.200	22	0.191	21	0.170	19	0.191	21	0.259	27	0.249	26
LA	0.183	20	0.189	21	0.235	26	0.236	26	0.201	21	0.196	21
OA	0.106	12	0.175	19	0.230	25	0.262	29	0.254	27	0.299	32
PA	0.253	28	0.182	20	0.190	21	0.136	15	0.207	22	0.179	19
SA	0.164	18	0.170	19	0.085	9	0.085	9	0.028	3	0.026	3
total	0.907		0.907		0.910		0.910		0.949		0.949	
AA	0.727	23	0.737	23	0.776	24	0.748	23				
LA	0.659	21	0.707	22	0.820	25	0.896	27				
OA	0.622	20	0.573	18	0.930	28	0.868	27				
PA	0.706	22	0.633	20	0.535	16	0.480	15				
SA	0.464	15	0.531	17	0.203	6	0.268	8				
total	3.18		3.18		3.26		3.26					
AA	6.22	32	5.63	29	5.52	29	5.39	28				
LA	4.71	24	4.94	25	6.25	32	5.91	31				
OA	2.51	13	2.89	15	3.76	20	4.16	22				
PA	3.20	16	3.64	19	2.35	12	2.62	14				
SA	2.93	15	2.46	13	1.37	7	1.18	6				
total	19.6		19.6		19.3		19.3					

[a] Experimental [FFA_{ui}] values were determined from three different mixtures (1:1:1:1:1, 20:25:30:15:10, and 25:20:33:19:3) of AA, LA, OA, PA, and SA by analyzing the measured probe responses with eq 4. The mixture ratios indicate the relative volume ratios of the FFA−BSA complexes used to prepare the mixtures (Experimental Procedures), and these are roughly the final [FFA_{ui}] ratios observed in the mixtures. Except for the 25:20:33:19:3 mixture (0.9 nM), three concentrations of total FFA_u (0.9, 3.2, and 20 nM) were used for each distribution. Model values of [FFA_{ui}] were calculated using the single-class model (eqs A4 and A6). Also shown is the fraction of each FFA_{ui} in the mixture (*X*).

Table 6: Estimated Experimental Errors in [FFA_{ui}] (percent)[a]

	20 nM	3 nM	0.9 nM		20 nM	3 nM	0.9 nM
AA	7	8	10	PA	3	4	10
LA	<1	3	4	SA	1	3	1
OA	6	16	30				

[a] Error estimates for [FFA_{ui}] were determined using a 1% error in *R* (see Experimental Procedures), and the results are shown for the mixtures of five fatty acids at three different concentrations from Table 5.

fluorescent probe in BSA-buffered stocks. Because all new probes were calibrated with ADIFAB2 to yield the same FFA_u concentration for each FFA−BSA complex, all probe-based [FFA_u] measurements are at least as reliable as those with ADIFAB2. We therefore expect the FFA_{ui} profile to be accurate no matter what binding model applies to BSA. Moreover, the remarkable agreement between the predicted and measured profiles strongly suggests that both measurement and model are correct. The model values for FFA_{ui} are predictions of eq A6 which are based upon the independently determined K_{di} values of Table 3.

A single-class binding model would seem to be inconsistent with published crystallographic structures of FFA−human serum albumin complexes in which seven chemically distinct binding sites are observed for long chain FFA (*37*). However, these structures reveal little about the binding affinities of these chemically distinct sites. NMR studies of ^{13}C-labeled FFA have revealed at least two to three distinct binding environments for BSA, even at the lowest FFA: albumin concentration ratios (*38*, *39*). However, it should be noted that NMR can detect binding interactions with FFA exchange rates of up to approximately 30 ms (*40*), extremely fine temporal resolution compared to that obtained with kinetic and binding measurements carried out on a 1−600 s time scale. We propose that our dissociation and binding measurements reflect an averaging of the microscopic parameters for FFA−BSA interactions. Thus, while our single-class model accurately predicts our experimentally determined FFA_u values, these results do not preclude the existence of multiple microscopic binding affinities.

The observed inverse relationship between BSA binding affinity and FFA solubility is consistent with our previous studies of binding of FFA to wild-type FABPs (*41*). In those studies, we showed that the total free energy change for the transfer of FFA from water to a relatively nonpolar FABP binding cavity reflected the sum of three free energy components: increased water entropy due to removal of hydrophobic FFA, decreased FFA entropy due to its immobilization in the binding pocket, and increased enthalpy from FFA−amino acid interactions. We concluded that during formation of FABP−FFA complexes, the FFA and water entropy changes tend to offset each other, resulting in a modest overall entropic change that essentially reflects FFA solubility. Thus, the overall free energy of binding is predominantly enthalpic, with a smaller but significant entropic component. The inverse relationship between FFA solubility and BSA binding affinity presented here may also reflect the contribution of a net positive entropy change in which the increase in water entropy is partially compensated by the FFA entropy loss upon binding to BSA.

FFA_u Profiling. To our knowledge, no other method has been reported for determining the FFA_u distribution in a mixture of FFA. Although methods for measuring the distribution of total (albumin bound and unbound) FFA exist, this profile differs considerably from the FFA_{ui} profile because of differences in FFA−BSA binding affinities. This difference is illustrated in Table 7 where the measured and model-predicted FFA_u distributions are shown with the predicted and experimentally determined total FFA distributions for two of the mixtures of Table 5. These results reveal, for example, that similar [FFA_u] values for SA and AA can be achieved only when the total SA concentration is

Table 7: FFA_u and Total FFA Distributions of Two Mixtures of Five Fatty Acids with BSA[a]

	1:1:1:1:1								20:25:30:15:10							
	experiment				model				experiment				model			
	$[FFA_u]$ (nM)	X (%)	total [FFA] (μM)	X (%)	$[FFA_u]$ (nM)	X (%)	total [FFA] (μM)	X (%)	$[FFA_u]$ (nM)	X (%)	total [FFA] (μM)	X (%)	$[FFA_u]$ (nM)	X (%)	total [FFA] (μM)	X (%)
AA	0.73	23	115	10	0.74	23	122	11	0.78	24	115	11	0.75	23	124	11
LA	0.66	21	169	15	0.71	22	171	15	0.82	25	212	20	0.90	27	217	20
OA	0.62	20	267	24	0.57	18	262	24	0.93	28	400	37	0.87	27	406	38
PA	0.71	2	240	21	0.63	20	219	20	0.54	16	180	17	0.48	15	167	15
SA	0.46	15	330	29	0.53	17	331	30	0.20	6	165	15	0.27	8	168	15
total	3.2		1121		3.2		1108		3.3		1072		3.3		1082	

[a] Experimental values of the total FFA profiles were determined from the amount of FFA that was used to make each FFA−BSA complex. The mixture ratios indicate the relative volume ratios of the FFA−BSA complexes used to prepare the mixtures (Experimental Procedures), and these are roughly the $[FFA_{ui}]$ ratios observed in the mixtures. (Note that the total FFA concentrations in Table 7 are the concentrations before the mixtures were diluted 100-fold in measurement buffer.) Model values of the total FFA profiles were calculated from the single-class BSA binding model (eq A6).

substantially higher than the total AA concentration, as expected from the difference in SA and AA binding affinities.

In addition to its greater physiologic relevance, the determination of the FFA_u profile has a number of important advantages over the total distribution methods, especially for biologic fluids such as blood plasma. FFA_u profiling using the fluorescent probes, for example, in blood plasma, requires little sample preparation. In contrast, measuring the total FFA distribution requires extensive procedures for extracting and separating the lipid components using organic solvents that can themselves alter the FFA distribution. Probe-based measurements require less sample because the measurements are performed directly in 100-fold diluted plasma (*20, 27*) and the measurements are amenable to high-throughput techniques such as fluorescent scanning in multiwell plates. On the other hand, probe specificity must be carefully investigated to account for potential interferents in biologic fluids. These and other issues are being investigated in our ongoing efforts to use these and other probes to help distinguish different disease states in human blood specimens.

APPENDIX

A Model for BSA−Fatty Acid Interactions. Our probe-based method is currently the only means for determining the FFA_u distribution of a mixture comprising multiple FFA in equilibrium with BSA. We have therefore developed a simplified FFA−BSA binding model for verifying our experimentally determined FFA_u distributions. We have assumed that the binding reactions of n different types of FFA with albumin molecules containing M binding sites is reversible and can be represented by the following set of reactions:

$$\{[A_f] + [FFA_{ui}] \leftrightarrows [A_{bi}]\} \tag{A1}$$

where $[A_f]$ is the concentration of free albumin sites, $[FFA_{ui}]$ is the concentration of unbound FFA of type i, and $[A_{bi}]$ is the concentration of albumin sites bound with species i. We made the additional assumptions that for each type of FFA all M binding sites are independent and have equal affinities.

According to this model, the albumin dissociation constant (K_{di}^a) for FFA of type i binding to each of the M sites is

$$K_{di}^a = \frac{[A_f][FFA_{ui}]}{[A_{bi}]} \tag{A2}$$

The total albumin (protein) concentration $[A_t]$ can be expressed in terms of the concentrations of free and bound sites as

$$[A_t] = \frac{1}{M}([A_f] + \sum_{i=1}^{n}[A_{bi}]) \tag{A3}$$

Equations A2 and A3 together with the relation $[A_{bi}] = [FA_{ti}] - [FFA_{ui}]$, where FA_{ti} is the total FFA of type i, yield eq A4 which can be used to solve for $[A_f]$ in terms of the known quantities $[FA_{ti}]$, $[A_t]$, and K_{di}^a

$$[A_t] = \frac{[A_f]}{M}\left(1 + \sum_{i=1}^{n}\frac{[FA_{ti}]}{K_{di}^a + [A_f]}\right) \tag{A4}$$

where $[FA_{ti}]$ and $[A_t]$ were determined from the concentration of the fatty acid and albumin stocks, respectively.

The K_{di}^a values were obtained from measurements of single-FFA binding isotherms by expressing the concentration of albumin-bound FFA ($[A_b]$) as a function of FFA_u according to

$$\frac{[A_b]}{[A_t]} = \frac{M[FFA_u]}{K_d^a + [FFA_u]} \tag{A5}$$

A nonlinear fit to eq A5 was used to determine K_{di}^a. We chose not to use a Scatchard analysis because the most relevant region of the binding isotherm for this study is at small FFA:albumin ratios and the Scatchard transformation generates large uncertainties in this region (*42*). MLAB, a mathematical and statistical modeling program, was used to solve eq A4 numerically for $[A_f]$, and the $[FFA_{ui}]$ distribution was then calculated from eq A6 as

$$[FFA_{ui}] = \frac{K_{di}^a[FA_{ti}]}{[A_f] + K_{di}^a} \tag{A6}$$

A simple analytical solution for the $[FFA_{ui}]$ distribution that provides an approximation valid under typical physiologic conditions can be obtained. Because the albumin concentrations are on the order of micromolar and binding affinities are in the nanomolar range, $[A_f] \gg K_{di}^a$ and eqs A4 and A6 can be reduced to eqs A7 and A8, respectively. The resulting

equations can be combined to give the approximate $[FFA_{ui}]$ profile (A9).

$$[A_t] \approx \frac{1}{M}([A_f] + [FA_t]) \quad \text{(A7)}$$

$$[FFA_{ui}] \approx \frac{K^a_{di}[FA_{ti}]}{[A_f]} \quad \text{(A8)}$$

$$[FFA_{ui}] \approx \frac{K^a_{di}[FA_{ti}]}{M[A_t] - [FA_t]} \quad \text{(A9)}$$

Equation A9 predicts an $[FFA_{ui}]$ distribution that is within 0.01% of the values computed using eqs A4 and A6 under most physiologic conditions where the high-affinity FFA binding sites on albumin are rarely saturated. If only the relative amount of each FFA ($\beta_i = [FA_{ti}]/[FA_t]$) is known, the relative amount of each unbound FFA ($\alpha_i = [FFA_{ui}]/[FFA_u]$) can be determined from the albumin dissociation constants for each FFA (eq A10).

$$\alpha_i = \frac{\beta_i K^a_{di}}{\sum_{i=1}^{n} \beta_i K^a_{di}} \quad \text{(A10)}$$

REFERENCES

1. Goodacre, R. (2005) Metabolomics: The way forward, *Metabolomics 1*, 1−2.
2. Sorrentino, D., Robinson, R. B., Kiang, C. L., and Berk, P. D. (1989) At physiologic albumin/oleate concentrations oleate uptake by isolated hepatocytes, cardiac myocytes, and adipocytes is a saturable function of the unbound oleate concentration, *J. Clin. Invest. 84*, 1325−1333.
3. Cupp, D., Kampf, J. P., and Kleinfeld, A. M. (2004) Fatty acid: albumin complexes and the determination of the transport of long chain free fatty acid across membranes, *Biochemistry 43*, 4473−4481.
4. Kampf, J. P., and Kleinfeld, A. M. (2004) Fatty acid transport in adipocytes monitored by imaging intracellular free fatty acid levels, *J. Biol. Chem. 279*, 35775−35780.
5. Richieri, G. V., Anel, A., and Kleinfeld, A. M. (1993) Interactions of long chain fatty acids and albumin: Determination of free fatty acid levels using the fluorescent probe ADIFAB, *Biochemistry 32*, 7574−7580.
6. Richieri, G. V., Ogata, R. T., and Kleinfeld, A. M. (1994) Equilibrium constants for the binding of fatty acids with fatty acid binding proteins from adipocyte, intestine, heart, and liver, measured with the fluorescence probe ADIFAB, *J. Biol. Chem. 269*, 23918−23930.
7. Apple, F. S., Kleinfeld, A. M., and Adams, J. E. (2004) Unbound Free Fatty Acid Concentrations Are Increased in Cardiac Ischemia, *Clin. Proteomics 1*, 41−44.
8. Poitout, V. (2003) The ins and outs of fatty acids on the pancreatic β cell, *Trends Endocrinol. Metab. 14*, 201−203.
9. Kleinfeld, A. M., and Okada, C. (2005) Free fatty acid release from human breast cancer tissue inhibits cytotoxic T lymphocyte-mediated killing, *J. Lipid Res. 46*, 1983−1990.
10. Yli-Jama, P., Meyer, H. E., Ringstad, J., and Pedersen, J. I. (2002) Serum free fatty acid pattern and risk of myocardial infarction: A case-control study, *J. Intern. Med. 251*, 19−28.
11. de Vries, J. E., Vork, M. M., Roemen, T. H., De Jong, Y. F., Cleutjens, J. P., van der Vusse, G. J., and van Bilsen, M. (1997) Saturated but not mono-unsaturated fatty acids induce apoptotic cell death in neonatal rat ventricular myocytes, *J. Lipid Res. 38*, 1384−1394.
12. Listenberger, L. L., Ory, D. S., and Schaffer, J. E. (2001) Palmitate-induced apoptosis can occur through a ceramide-independent pathway, *J. Biol. Chem. 276*, 14890−14895.
13. Hickson-Bick, D. L., Sparagna, G. C., Buja, L. M., and McMillin, J. B. (2002) Palmitate-induced apoptosis in neonatal cardiomyocytes is not dependent on the generation of ROS, *Am. J. Physiol. 282*, H656−H664.
14. Richieri, G. V., and Kleinfeld, A. M. (1989) Free fatty acid perturbation of transmembrane signaling in cytotoxic T lymphocytes, *J. Immunol. 143*, 2302−2310.
15. Lorentzen, B., Drevon, C. A., Endresen, M. J., and Henriksen, T. (1995) Fatty acid pattern of esterified and free fatty acids in sera of women with normal and pre-eclamptic pregnancy, *Br. J. Obstet. Gynaecol. 102*, 530−537.
16. Rodriguez de Turco, E. B., Belayev, L., Liu, Y., Busto, R., Parkins, N., Bazan, N. G., and Ginsberg, M. D. (2002) Systemic fatty acid responses to transient focal cerebral ischemia: Influence of neuroprotectant therapy with human albumin, *J. Neurochem. 83*, 515−524.
17. Yli-Jama, P., Seljeflot, I., Meyer, H. E., Hjerkinn, E. M., Arnesen, H., and Pedersen, J. I. (2002) Serum non-esterified very long-chain PUFA are associated with markers of endothelial dysfunction, *Atherosclerosis 164*, 275−281.
18. Freedman, S. D., Blanco, P. G., Zaman, M. M., Shea, J. C., Ollero, M., Hopper, I. K., Weed, D. A., Gelrud, A., Regan, M. M., Laposata, M., Alvarez, J. G., and O'Sullivan, B. P. (2004) Association of cystic fibrosis with abnormalities in fatty acid metabolism, *N. Engl. J. Med. 350*, 560−569.
19. Spector, A. A. (1975) Fatty acid binding to plasma albumin, *J. Lipid Res. 16*, 165−179.
20. Richieri, G. V., and Kleinfeld, A. M. (1995) Unbound free fatty acid levels in human serum, *J. Lipid Res. 36*, 229−240.
21. Richieri, G. V., Ogata, R. T., and Kleinfeld, A. M. (1992) A fluorescently labeled intestinal fatty acid binding protein: Interactions with fatty acids and its use in monitoring free fatty acids, *J. Biol. Chem. 267*, 23495−23501.
22. Richieri, G. V., Ogata, R. T., and Kleinfeld, A. M. (1996) Kinetics of fatty acid interactions with fatty acid binding proteins from adipocyte, heart, and intestine, *J. Biol. Chem. 271*, 11291−11300.
23. Ho, S. N., Hunt, H. D., Horton, R. M., Pullen, J. K., and Pease, L. R. (1989) Site-directed mutagenesis by overlap extension using the polymerase chain reaction, *Gene 77*, 51−59.
24. Bradford, M. M. (1976) A rapid and sensitive method for the quantitation of microgram quantities of protein utilizing the principle of protein-dye binding, *Anal. Biochem. 72*, 248−254.
25. Kampf, J. P., Cupp, D., and Kleinfeld, A. M. (2006) Different mechanisms of free fatty acid flip-flop and dissociation revealed by temperature and molecular species dependence of transport across lipid vesicles, *J. Biol. Chem.* (in press).
26. Yuvienco, J. M. S., Dizon, E. C., Kleinfeld, A. M., Anwar, M., Hiatt, M., and Hegyi, T. (2005) Umbilical cord unbound free fatty acid concentration and low Apgar score, *Am. J. Perinatol. 22*, 429−436.
27. Richieri, G. V., Ogata, R. T., and Kleinfeld, A. M. (1999) The measurement of free fatty acid concentration with the fluorescent probe ADIFAB: A practical guide for the use of the ADIFAB probe, *Mol. Cell. Biochem. 192*, 87−94.
28. Richieri, G. V., Low, P. J., Ogata, R. T., and Kleinfeld, A. M. (1997) Mutants of rat intestinal fatty acid binding protein illustrate the critical role played by enthalpy-entropy compensation in ligand binding, *J. Biol. Chem. 272*, 16737−16740.
29. Richieri, G. V., Low, P. J., Ogata, R. T., and Kleinfeld, A. M. (1998) Thermodynamics of fatty acid binding to engineered mutants of the adipocyte and intestinal fatty acid binding proteins, *J. Biol. Chem. 273*, 7397−7405.
30. Spector, A. A., Fletcher, J. E., and Ashbrook, J. D. (1971) Analysis of long-chain free fatty acid binding to bovine serum albumin by determination of stepwise binding constants, *Biochemistry 10*, 3229−3232.
31. Bojesen, I. N., and Bojesen, E. (1992) exchange efflux of [^{3}H]-palmitate from human red cell ghost to bovine serum albumin in buffer. Effects of medium volume and concentration of bovine serum albumin, *Biochim. Biophys. Acta 2736*, 185−196.
32. Rose, H., Conventz, M., Fischer, Y., Jungling, E., Hennecke, T., and Kammermeier, H. (1994) Long-chain fatty acid-binding to albumin: Re-evaluation with directly measured concentrations, *Biochim. Biophys. Acta 1215*, 321−326.
33. Bojesen, I. N., and Bojesen, E. (1994) Binding of arachidonate and oleate to bovine serum albumin, *J. Lipid Res. 35*, 770−778.
34. Bojesen, I. N., and Bojesen, E. (1996) Albumin binding of long chain fatty acids: Thermodynamics and kinetics, *J. Phys. Chem. 100*, 17981−17985.

35. Elmadhoun, B. M., Wang, G. Q., Templeton, J. F., and Burczynski, F. J. (1998) Binding of [^{3}H]palmitate to BSA, *Am. J. Physiol. 275*, G638−G644.
36. Demant, E. J. F., Richieri, G. V., and Kleinfeld, A. M. (2002) Stopped-flow kinetic analysis of long-chain fatty acid dissociation from bovine serum albumin, *Biochem. J. 363*, 809−815.
37. Petitpas, I., Grune, T., Bhattacharya, A. A., and Curry, S. (2001) Crystal structures of human serum albumin complexed with monounsaturated and polyunsaturated fatty acids, *J. Mol. Biol. 314*, 955−960.
38. Parks, J. S., Cistola, D. P., Small, D. M., and Hamilton, J. A. (1983) Interactions of the carboxyl group of oleic acid with bovine serum albumin: A ^{13}C NMR study, *J. Biol. Chem. 258*, 9262−9269.
39. Cistola, D. P., Small, D. M., and Hamilton, J. A. (1987) Carbon ^{13} NMR studies of saturated fatty acids bound to bovine serum albumin: The filling of individual fatty acid binding sites, *J. Biol. Chem. 262*, 10971−10979.
40. Hamilton, J. A., and Cistola, D. P. (1986) Transfer of oleic acid between albumin and phospholipid vesicles, *Proc. Natl. Acad. Sci. U.S.A. 83*, 82−86.
41. Richieri, G. V., Ogata, R. T., and Kleinfeld, A. M. (1995) Thermodynamics of fatty acid binding to fatty acid-binding proteins and fatty acid partition between water and membranes measured using the fluorescent probe ADIFAB, *J. Biol. Chem. 270*, 15076−15084.
42. Munson, P. J., and Rodbard, D. (1983) Number of receptor sites from Scatchard and Klotz graphs: A constructive critique, *Science 220*, 979−981.

BI060703E